



Application of Unstructured T-spline Continuity Elevation Algorithm in Surface Merging

Chao Zuo¹ , Gang Zhao^{1,2}  and Wei Wang^{1,3} 

¹School of Mechanical Engineering and Automation, Beihang University, zuocbuaa@163.com

²Key Laboratory of Aeronautics Smart Manufacturing, Ministry of Industry and Information Technology, zhaog@buaa.edu.cn

³Beijing Engineering Technological Research Center of High-Efficient and Green CNC Machining Process and Equipment, jrrt@buaa.edu.cn

Corresponding author: Wei Wang, jrrt@buaa.edu.cn

Abstract. In CAGD, the emergence of unstructured T-splines enables a single surface to express a complex model, and a water-tight surface is also obtainable through T-splines in the surface merging. However, the presence of extraordinary points has some impact on the surface: only C^0 continuity can be obtained around the extraordinary points and the traditional local refinement algorithm can't be used in the vicinity of the extraordinary points. To enhance the continuity, based on the D-Patch framework and basis function truncation, the design space and analysis space continuity enhancement algorithms are developed in this paper. Certain use cases of merging multiple surfaces into one unstructured T-spline surface are demonstrated, then the algorithms are executed so that the spoke edges can have C^1 continuity. Rhino's zebra pattern analysis proves that the spoke edges have C^1 continuity, which can lay a sound foundation for isogeometric analysis.

Keywords: Unstructured T-spline, Extraordinary Point, Continuity Enhancement, Bézier Extraction.

DOI: <https://doi.org/10.14733/cadaps.2023.540-556>

1 INTRODUCTION

In CAGD, B-spline has been used to describe the free-form shapes in miscellaneous occasions and is widely used in modeling. With the introduction of weight, B-spline can be upgraded as NURBS, then primary analytic surfaces such as spherical and cylindrical surfaces can be represented. The unified expression of free surfaces as well as primary analytic surfaces by NURBS has long become the backbone of CAD software, but there are still the following drawbacks in existing systems: (1) a single surface cannot express complex model; (2) it is difficult to obtain watertight geometries in surface merging; (3) for the limitation of the rectangular grid, a large number of superfluous

control points will be introduced during local refinement. To overcome these drawbacks, T-spline was proposed by Sederberg et al.^[10], of which the T-junction breaks through the limitation of the control mesh's rectangular topology, so (2) and (3) of the above drawbacks are annihilated. By introducing extraordinary points into T-spline, with which the T-spline is called as unstructured T-spline, (1) of the above drawbacks is also relieved. But unstructured T-spline results in new problems: (1) only C^0 continuity can be obtained around the extraordinary point; (2) the traditional local refinement algorithm^[9] cannot be used in the vicinity of the extraordinary points. These problems may affect the accuracy of modeling and analysis, even make T-spline fail to meet some design situations with high continuity requirements.

The T-spline technology is promising if it fully accommodates the requirement of Isogeometric Analysis (IGA). While the C^0 continuity limitation around the extraordinary point is not wanted because one of IGA's advantages is that it offers a framework of high-order analysis. In order to closely combine T-spline modeling with IGA, in this paper, we demonstrate certain use cases of merging multiple NURBS surfaces into one unstructured T-spline surface and then elevate the continuity around extraordinary points, after which the IGA can be implemented. This approach can effectively exploit the potential of unstructured T-spline technology in modeling as well as in analysis, and promote the possible advent of a new design pattern based on integrating geometric modeling and performance evaluation more closely.

2 T-SPLINE FOUNDATION

The T-spline uses a point-spline approach to define the surface. Each control point is associated with a spline basis function, and the T-spline surface is obtained by multiplying the control points' coordinates with corresponding spline basis functions then accumulating them. NURBS has control points in strict rows and columns. T-spline introduces T-junctions based on NURBS, so it can be regarded as a generalization of NURBS, and is also known as structured T-spline. In the structured T-spline, the existence of the T-junctions transcends the limitation of the rectangular parameter domain, resulting in "T"-shaped nodes inside the T-mesh, and fewer control points are introduced during the local refinement or surface merging. The problem of gaps in NURBS surface merging can be solved by T-spline's arbitrary topology parameter domain, which enhances the continuity in surface merging.

Unlike NURBS basis functions which are defined based on knot vectors, T-spline basis functions are defined based on knot interval vectors, which are obtained from T-mesh. The knot interval vector is a relative vector based on the coordinate system, while the knot vector is an absolute vector based on the same coordinate system. The knot interval reflects the distance between two adjacent knots, so the knot vector and knot interval vector can be converted to each other. Assuming a U-direction knot vector $U = [u_0, u_1, u_2, u_3, u_4] = [0, 1, 2, 3, 5]$ as example, it can be converted into a U-direction knot interval vector $D = [d_0, d_1, d_2, d_3] = [u_1 - u_0, u_2 - u_1, u_3 - u_2, u_4 - u_3] = [1, 1, 1, 2]$; assuming a U-direction knot interval vector $D = [d_0, d_1, d_2, d_3]$ as example, according to spline basis function center coordinates (u, v) , the U-direction knot vector can be obtained as: $U = [u - d_0 - d_1, u - d_1, u, u + d_2, u + d_2 + d_3]$. When given knot interval vectors $[d_0, d_1, d_2, d_3] \times [e_0, e_1, e_2, e_3]$, they can be converted to knot vectors, and the bi-cubic spline basis function $B_i(u, v)$ in T-spline is equivalent to the B-spline basis function, which can be constructed from the associated knot vectors. The following discussion is based on uniform knot interval, and the specific method to obtain knot interval vectors is detailed in [10].

The unstructured T-spline introduces extraordinary points into the structured T-spline, which solves the problem that one single structured T-spline surface cannot express a complex model. The valence, denoted by μ , is the number of edges that depart from a certain point. In

unstructured T-spline, extraordinary points are those internal control points with $\mu \neq 4$ that are not T-junctions, or boundary control points with $\mu > 3$. Spoke edges are edges emanating from the extraordinary point. Extraordinary points will affect the surrounding faces and control points. For the convenience of subsequent discussion, we classify the related faces and control points into different categories: (1) 1-ring faces are faces that are in contact with extraordinary points, also called irregular faces; n-ring faces are faces that are in contact with (n-1)-ring faces and do not belong to (n-2)-ring faces. 2-ring faces are also referred as transition faces, and the faces that do not belong to 1-ring or 2-ring faces are called regular faces. N-disk faces of an extraordinary point are defined as the set containing all its 1, 2, ..., n-ring faces, as shown in Figure 1(a). (2) 0-ring points are extraordinary points, also called irregular control points; n-ring points are control points on n-ring faces that do not belong to (n-1)-ring points. 1-ring points are also referred as transition control points, and the control points that do not belong to 1-ring points or 0-ring points are called regular control points. N-disk points of an extraordinary point are defined as the set of points containing all its 0, 1, ..., n-ring points, as shown in Figure 1(b).

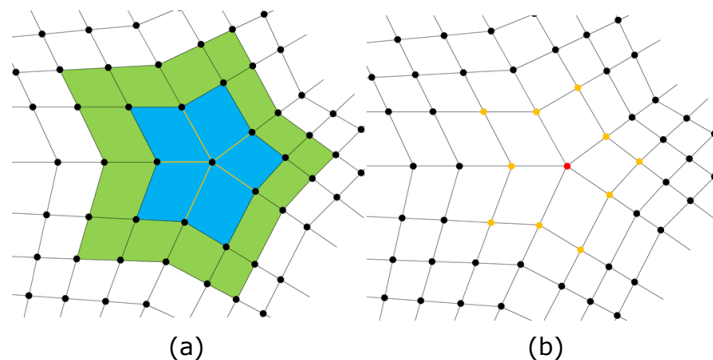


Figure 1: (a) The classification of faces, (b) The classification of control points. The irregular faces, transition faces, and regular faces are marked with blue, light green and white, respectively; irregular points, transition points, and regular points are marked with red, orange and black, respectively; spoke edges are represented by yellow lines in (a).

T-splines are not naturally suitable for IGA, and certain restrictions are imposed on T-splines to make them suitable for IGA. This subset of T-splines is called analysis-suitable T-splines (ASTS), and it is defined on an admissible T-mesh, which is defined by the T-junctions and the T-junction extensions^{[3][7]}. Here, the concept of the T-junction extension is given: T-junction extension includes face extension and edge extension. Face extension is a line segment that starts at the T-junction and emits rays in the direction of the missing edge until it intersects 2 edges. Edge extension is a line segment that starts at T-junction and emits rays in the opposite direction of the face extension until it intersects 1 edge. Figure 2(b) gives an example of T-junction extensions. One-bay face extension is a line segment that starts at T-junction and emits rays in the direction of the face extension until it intersects 1 edge. According to the concept of Toshniwal et al.^{[8][11]}, the admissible T-mesh containing extraordinary points is now defined, as shown in Figure 2(a):

- No T-junction extensions intersect
- No one-bay face extension exists in the 3-disk faces of an extraordinary point
- No extraordinary points belong to the 3-disk points of other extraordinary points
- No extraordinary points belong to the 2-disk points of the T-mesh boundary

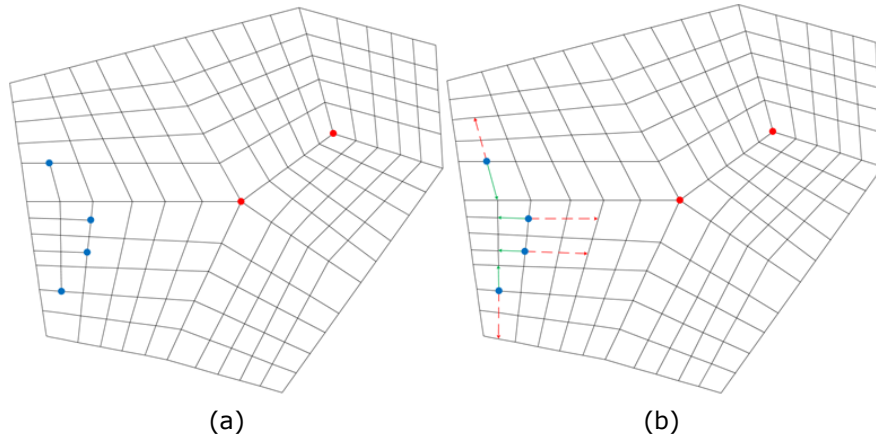


Figure 2: (a) The admissible T-mesh, (b) The T-junction extension in T-mesh. The red control points are the extraordinary points, and the blue points are the T-junctions; the red dashed line segment represents the face extension, and the green line segment represents the edge extension.

The analysis model in finite element analysis can only approximate the geometric model. However, IGA directly uses the geometric model as the analysis model, which circumvents the mesh generation and avoids the model conversion work. By applying ASTS to IGA, a single surface can be used to represent the complex model, and the model has the ability of local refinement. But there are still some limitations: the spoke edges of the extraordinary point only have C^0 continuity, which makes the Kirchhoff-Love shell analysis impossible, and the traditional refinement algorithm cannot be used near the 2-disk faces of the extraordinary points. Geometric modeling only considers how to construct the shape features, while IGA needs to consider the accuracy of the analysis, geometric invariance when refinement and the stability of the calculation. So IGA has additional requirements compared to geometric modeling. Therefore, the design space and the analysis space should be established respectively, and the basic properties of the design space and the analysis space are linear independence of basis functions, local support of basis functions, the partition of unity of the basis functions, as well as the non-negativity of basis functions, besides which there are some additional properties^[11]:

Design space

- Local refinement capability
- C^1 continuity everywhere

Analysis Space

- Local refinement capability
- C^1 continuity everywhere
- The sub-spline space generated by the refinement should keep the geometry unchanged and maintain the optimal convergence rate of partial differential equations

To meet these requirements of analysis space, each irregular face introduces four face points and forms the analysis space^[11]. Each face point is associated with a face point basis function. The face points can be calculated by Equation (2.1) - (2.4) and the distribution of the face points is shown in Figure 3.

$$Q_5^i = \frac{4}{9}P_1 + \frac{2}{9}P_2 + \frac{2}{9}P_3 + \frac{1}{9}P_4 \quad (2.1)$$

$$Q_6^i = \frac{2}{9}P_1 + \frac{4}{9}P_2 + \frac{1}{9}P_3 + \frac{2}{9}P_4 \quad (2.2)$$

$$Q_9^i = \frac{2}{9}P_1 + \frac{1}{9}P_2 + \frac{4}{9}P_3 + \frac{2}{9}P_4 \quad (2.3)$$

$$Q_{10}^i = \frac{1}{9}P_1 + \frac{2}{9}P_2 + \frac{2}{9}P_3 + \frac{4}{9}P_4 \quad (2.4)$$

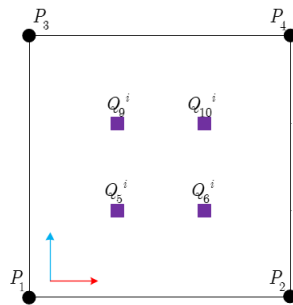


Figure 3: The spline control points P and face points Q^i of the irregular face in the local coordinate system.

The original T-mesh and its control points are called the design space. Figure 4(a) gives an example of control points in the design space, and Figure 4(b) shows the corresponding example of control points in the analysis space.

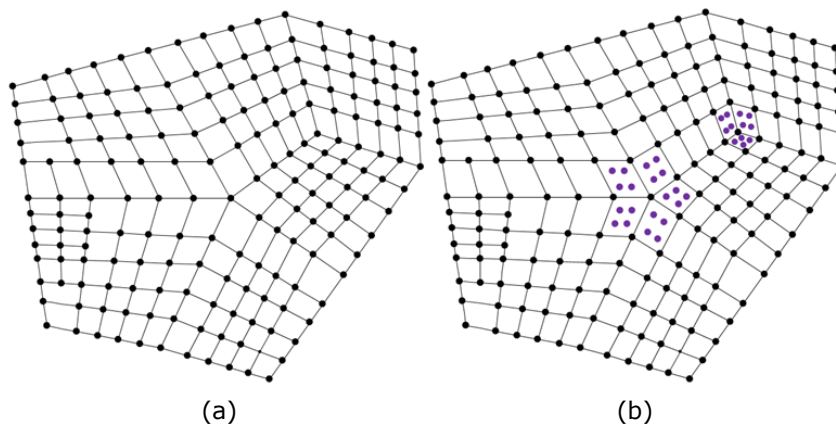


Figure 4: (a) Control points in the design space, (b) Control points in the analysis space. The black points are spline control points, and the purple points are face points, respectively. Compared with the design space, in the analysis space, each irregular face contains four face points. The classification of faces and control points is the same in both spaces, notice that face points do not participate in the above classification.

3 BÉZIER EXTRACTION

We assume that the reader is familiar with Bézier extraction. In Figure 5(c), the face to be analyzed is marked in yellow, and the face points that affect the face are marked with brown. Next,

we will briefly describe how to use face points to calculate Bézier control points so the model can be used for IGA. Bézier control points can be divided into three types: Bézier face points, Bézier edge points, and Bézier corner points. The face points of this face are the Bézier face points; the Bézier edge points are calculated according to Equation (3.1) - (3.2), as shown in Figure 5(a); the Bézier corner points are calculated according to Equation (3.3), as shown in Figure 5(b). The final result is shown in Figure 5(c).

$$Q_1^{i+1} = Q_4^i = \frac{1}{2}Q_5^{i+1} + \frac{1}{2}Q_5^i \tag{3.1}$$

$$Q_2^{i+1} = Q_8^i = \frac{1}{2}Q_6^{i+1} + \frac{1}{2}Q_9^i \tag{3.2}$$

$$Q_0 = \frac{1}{\mu}(Q_5^i + Q_5^{i+1} + \dots + Q_5^{i+\mu-1}) \tag{3.3}$$

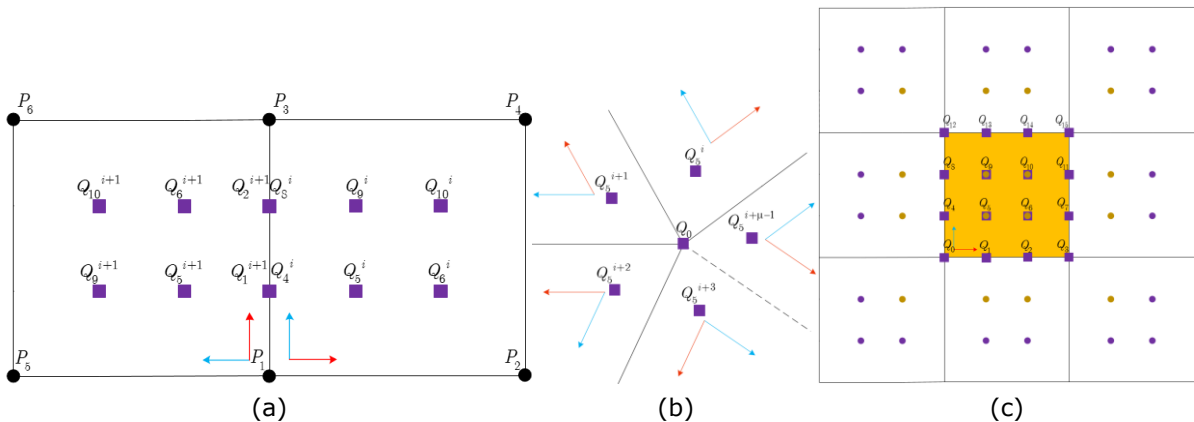


Figure 5: (a) The correspondence between Bézier edge points and face points, (b) The correspondence between Bézier corner points and face points, (c) Affecting face points and Bézier control points of the yellow face. The brown face points are face points that affect the face, others are the irrelevant face points, and the square points are Bézier control points of the yellow face, of which the central four face points also belong to face points. The Bézier face points can be calculated according to Figure 3. The Bézier edge points and Bézier corner points can be calculated according to Figure 5(a), and Figure 5(b) respectively.

According to Bézier extraction, T-spline control points P can be transformed into Bézier control points Q^0 : $Q^0 = EP$, where E is called the extraction matrix^{[1][2][6]}. The transpose matrix E^T of E , called extraction operator M , reflects the transformation relationship between Bernstein basis functions $B^0(u,v)$ and spline basis functions $B^V(u,v)$, i.e., $B^V(u,v) = MB^0(u,v)$, which indicates that each row vector of M can define a spline basis function, and the row vector is called extraction coefficient. In fact, the extraction coefficient reflects the corresponding Bézier control points, and modifying the extraction coefficient is equivalent to modifying the Bézier control points.

The extraction coefficient can define a spline basis function, which is obtained by a linear combination of Bernstein basis functions. The following will demonstrate how to obtain the extraction coefficient. In Figure 6(a), the face S to be analyzed is marked with yellow, the black points are the irrelevant face points, and other colored points are the face points that affect face S , which means that the colored points are the face points that contribute to the calculation of extraction coefficient. These colored points are divided into three categories (the face position face points, the edge position face points, and the corner position face points), represented by blue,

green and light green. The local coordinate system of the face S and the arrangement of the extraction coefficient is shown in Figure 6(b). Each face point has a face point basis function that corresponds to the three types of face points and can be obtained by the linear combination of Bernstein basis functions, as shown in Figure 7(a)-(c).

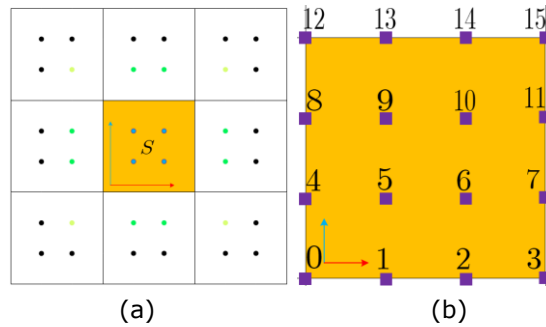


Figure 6: (a) Affecting face points, (b) The distribution of extraction coefficient for the current face. This face is marked in yellow, the black points are irrelevant face points, and the colored points are the face points that affect this face, among which the face position face points, the edge position face points, and the corner position face points are marked in blue, green, light green, respectively. (b) arranges the extraction coefficient of this face in the manner of u first and then v .

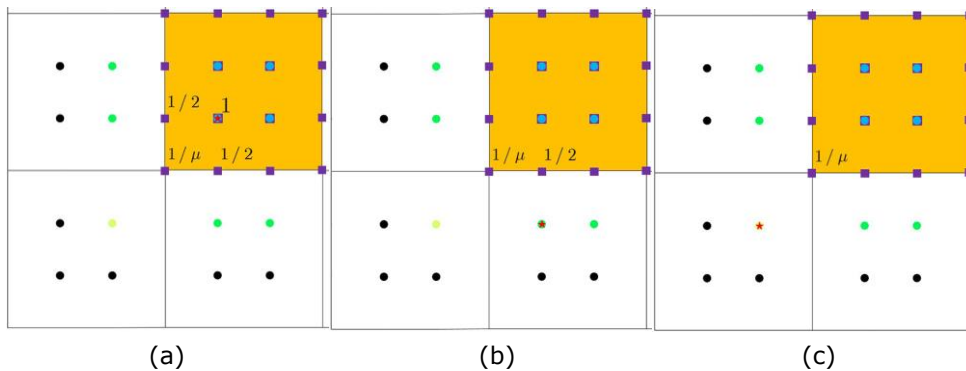


Figure 7: (a), (b), and (c) show the different corresponding relationships between Bernstein basis functions and face point basis functions. Three different types of face points (blue, green, and light green points) are included and the face point to be analyzed is the face point marked with a red pentagram. Each face point has a face point basis function. The Bernstein basis functions are represented by square points. Square points without notation on it represent the corresponding coefficients are 0.

Each spline basis function can be obtained by a linear combination of the face point basis functions of adjacent faces that contact this point^[2], the coefficient of each face point basis function is called the face point coefficient, as shown in Figure 8(a). For an upper right face in Figure 8(a), the local extraction coefficient of the face, as shown in Figure 8(b), is obtained by multiplying per face point coefficients $\left(Q_{10} = \frac{4}{9}, Q_{11} = \frac{2}{9}, Q_{14} = \frac{2}{9}, Q_{15} = \frac{1}{9} \right)$ and the coefficients $\left(\frac{1}{\mu}, \frac{1}{2}, \frac{1}{2}, 1 \right) \mu = 4$ in Figure 7(a) respectively. In Figure 8(b), for the four face point coefficients $Q_{10}, Q_{11}, Q_{14}, Q_{15}$ of the current face, we will briefly introduce how to obtain the local extraction coefficient: for the face point coefficient

$Q_{10} = \frac{4}{9}$, multiply it with the coefficients $\left(\frac{1}{\mu}, \frac{1}{2}, \frac{1}{2}, 1\right)$ $\mu = 4$ in Figure 7(a) to obtain the extraction coefficient of 0,1,4,5 position (the index is based on Figure 6(b)):

$$\left(0: Q_{10} * \frac{1}{\mu} = \frac{1}{9}, 1: Q_{10} * \frac{1}{2} = \frac{2}{9}, 4: Q_{10} * \frac{1}{2} = \frac{2}{9}, 5: Q_{10} * 1 = \frac{4}{9}\right) \tag{3.4}$$

Similarly, according to the face point coefficients $\left(Q_{11} = \frac{2}{9}, Q_{14} = \frac{2}{9}, Q_{15} = \frac{1}{9}\right)$, we can also obtain other extraction coefficient of 2,3,6,7, 8,9,12,13, and 10,11,14,15 positions respectively

$$\left\{ \begin{array}{l} 2: Q_{11} * \frac{1}{2} = \frac{1}{9}, 3: Q_{11} * \frac{1}{\mu} = \frac{1}{18}, 6: Q_{11} * 1 = \frac{2}{9}, 7: Q_{11} * \frac{1}{2} = \frac{1}{9} \\ 8: Q_{14} * \frac{1}{2} = \frac{1}{9}, 9: Q_{14} * 1 = \frac{2}{9}, 12: Q_{14} * \frac{1}{\mu} = \frac{1}{18}, 13: Q_{14} * \frac{1}{2} = \frac{1}{9} \\ 10: Q_{15} * 1 = \frac{1}{9}, 11: Q_{15} * \frac{1}{2} = \frac{1}{18}, 14: Q_{15} * \frac{1}{2} = \frac{1}{18}, 15: Q_{15} * \frac{1}{\mu} = \frac{1}{36} \end{array} \right. \tag{3.5}$$

Then the local extraction coefficient are $\left[\frac{1}{9} \frac{2}{9} \frac{1}{9} \frac{1}{18} \frac{2}{9} \frac{4}{9} \frac{2}{9} \frac{1}{9} \frac{1}{9} \frac{2}{9} \frac{1}{9} \frac{1}{18} \frac{1}{18} \frac{1}{9} \frac{1}{18} \frac{1}{36}\right]$. For

the spline basis function at P_i in Figure 8. Calculate the corresponding local extraction coefficients of the four adjacent faces respectively, and the global extraction coefficient, as shown in Figure 8(c), is obtained by combining four-set local extraction coefficients.

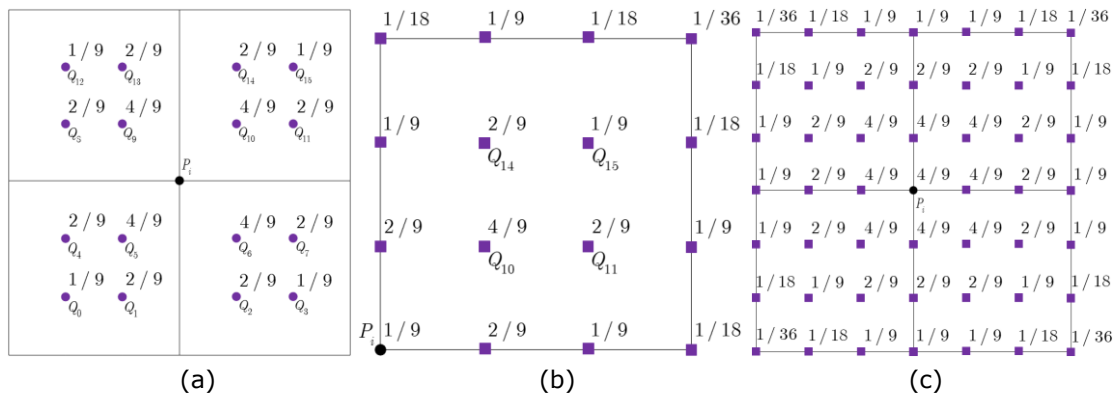


Figure 8: (a) The correspondence between the current spline basis function (at P_i) and the face point basis function of its adjacent faces, (b) Local extraction coefficient for an upper right face, (c) Global extraction coefficient of current spline basis function. The global extraction coefficient can be obtained by combining the local extraction coefficients of four faces.

There are three types of affecting spline control points of the face S in Figure 9(a), according to the positions of the three types, the global extraction coefficient can be converted into the extraction coefficient of this spline basis function, and the extraction coefficient is what we need, as shown in Figure 9(b)-(d) respectively. Take the green spline control point for example, among the global extraction coefficients of the corresponding spline basis function, only four extraction

coefficients $\left(\frac{1}{36} \quad \frac{1}{18} \quad \frac{1}{9} \quad \frac{1}{9}\right)$ in the upper left corner are projected on the face S , so the extraction coefficient of the spline basis function is $\left[\frac{1}{36} \quad \frac{1}{18} \quad \frac{1}{9} \quad \frac{1}{9} \quad 0 \quad 0\right]$.

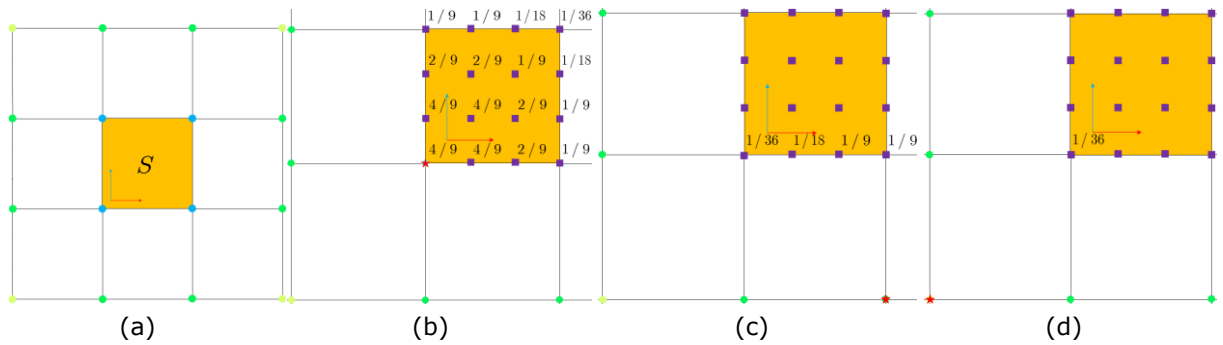


Figure 9: (a) Affecting spline control points of the face S , which can be divided into three types (blue, green, and light green); (b), (c), and (d) are the extraction coefficients corresponding to different types of spline basis functions (the control point to be analyzed is the point marked with a red pentagram), which can be obtained by the projection of the global extraction coefficients of the spline basis functions into the current face. Square points without notation on it represent the corresponding coefficients are 0.

4 SMOOTHING SPOKE EDGE

Based on the D-Patch framework^{[2][5][11]} and basis function truncation^[2], using a half-edge data structure to express T-spline surfaces, we take a split-smoother approach^[4] to achieve spoke edge smoothness for design space and analysis space, respectively. Unlike the direct modification of Bézier control points by Toshniwal D.^[11], for subsequent IGA, we modify the Bézier control points indirectly by modifying the extraction coefficients, resulting in continuity enhancement. Figure 10 shows the flowchart of the algorithm. The procedure can be described as follows.

(1) In the design space, the approach is used for irregular faces, and obtaining C^1 continuity crossing spoke edges. The approach is applied as:

- For an irregular face, we obtain all the spline basis functions that have support on this face and call them support basis functions.
- Obtain the extraction coefficient $(C_0^i, C_2^i, \dots, C_{15}^i) (i = 1, 2, \dots, \mu)$ defining a support basis function on each irregular face, arrange the extraction coefficient in the manner of Figure 6(b), and express them in the following form.

$$C^i = \begin{bmatrix} C_{12}^i & C_{13}^i & C_{14}^i & C_{15}^i \\ C_8^i & C_9^i & C_{10}^i & C_{11}^i \\ C_4^i & C_5^i & C_6^i & C_7^i \\ C_0^i & C_1^i & C_2^i & C_3^i \end{bmatrix} \tag{4.1}$$

- Perform a split of this extraction coefficient, then four new sets of extraction coefficients $C^{i,pq} = C_j^{i,pq} (i = 1, 2, \dots, \mu; j = 0, 1, \dots, 15; p, q = 0, 1)$ will be obtained

where

$$S_0 = \begin{bmatrix} 1 & 0 & 0 & 0 \\ \frac{1}{2} & \frac{1}{2} & 0 & 0 \\ \frac{1}{4} & \frac{1}{2} & \frac{1}{4} & 0 \\ \frac{1}{8} & \frac{3}{8} & \frac{3}{8} & \frac{1}{8} \end{bmatrix}, S_1 = \begin{bmatrix} \frac{1}{8} & \frac{3}{8} & \frac{3}{8} & \frac{1}{8} \\ 0 & \frac{1}{4} & \frac{1}{2} & \frac{1}{4} \\ 0 & 0 & \frac{1}{2} & \frac{1}{2} \\ 0 & 0 & 0 & 1 \end{bmatrix} \tag{4.3}$$

$$C^{i,pq} = S_p C^i (S_q)^T \tag{4.2}$$

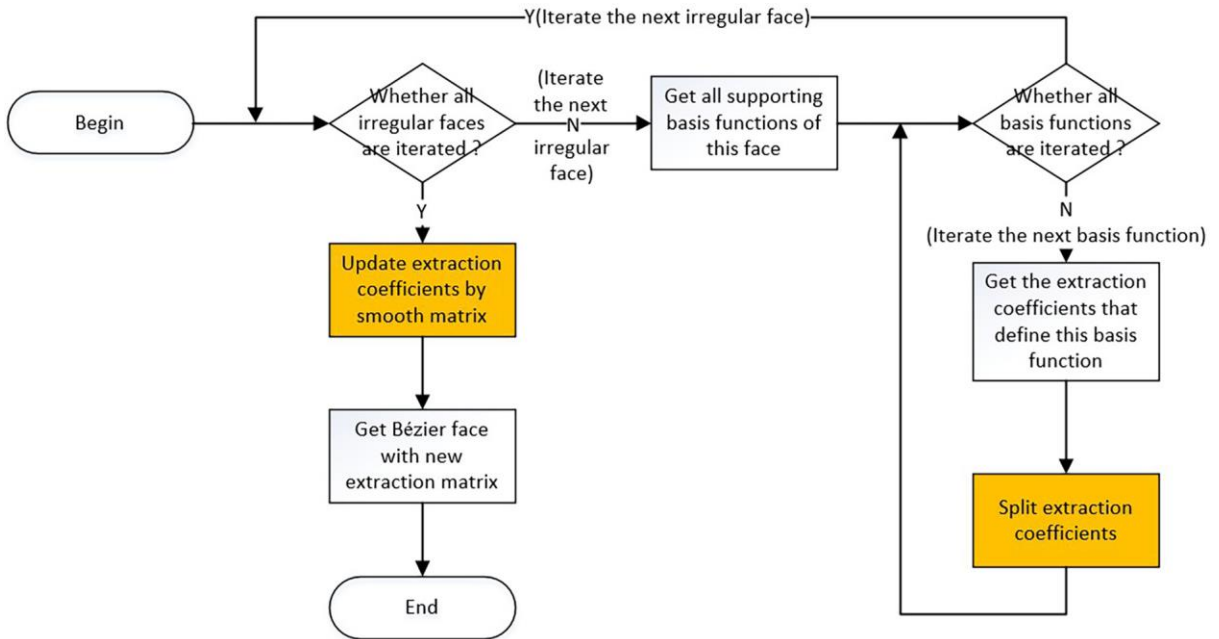


Figure 10: The flowchart of the split-smoothen approach

This can be regarded as using the de Casteljaou algorithm at $u = \frac{u_0}{2}, v = \frac{v_0}{2}$ (u_0 and v_0 represent the lengths of the U-direction and V-direction parameter edges of this face) of the parameter domain to split it into four sub-element domains, which are numbered as shown in Figure 11(b).

- Repeat the above two steps for each support basis function, then this face is split into four sub-faces. All irregular faces should be split, as shown in Figure 11(c).
- Modify the extraction coefficients $C_5^{i,00}, C_6^{i,00}, C_9^{i,00}$ using the Equation (4.4),

$$\begin{bmatrix} a_5 \\ a_6 \\ a_9 \end{bmatrix} = \Pi^+ \begin{bmatrix} A_5 \\ A_6 \\ A_9 \end{bmatrix} \tag{4.4}$$

where a_k and $A_k (k = 5, 6, 9)$ are column vectors of extraction coefficients with dimension μ , for example $A_5 = [C_5^{0,00}, C_5^{1,00}, \dots, C_5^{\mu-1,00}]^T$, and Π^+ is the smooth matrix :

$$\Pi^+ = \begin{bmatrix} \Pi_7^+ & \Pi_8^+ & \Pi_9^+ \\ \Pi_4^+ & \Pi_5^+ & \Pi_6^+ \\ \Pi_1^+ & \Pi_2^+ & \Pi_3^+ \end{bmatrix} \tag{4.5}$$

$$\Pi_i^+ = \begin{pmatrix} \Pi_{i,11}^+ & \dots & \Pi_{i,1\mu}^+ \\ \vdots & \ddots & \vdots \\ \Pi_{i,\mu 1}^+ & \dots & \Pi_{i,\mu\mu}^+ \end{pmatrix} \tag{4.6}$$

$$\Pi_{i,jk}^+ = p_i^{(j-k)\% \mu} \tag{4.7}$$

$$\begin{cases} p_1^j = p_4^j = p_7^j = 0 \\ p_2^j = \frac{1}{2\mu}(1 + \cos(2\psi - j\varphi)) \\ p_3^j = p_5^j = \frac{1}{2\mu}(1 + \cos(j\varphi)) \\ p_6^j = \frac{1}{2\mu}(1 + \cos(2\psi + j\varphi)) \\ p_8^j = p_9^j = \frac{1}{2\mu} \end{cases} \tag{4.8}$$

$$p_1^j = p_4^{-j}, p_2^j = p_6^{-j}, p_3^j = p_5^{-j}, p_7^j = p_7^{-j}, p_8^j = p_9^{-j} \tag{4.9}$$

where the dimension of Π^+ is $3\mu \times 3\mu$, $\varphi = 2\frac{\pi}{\mu}$, $\psi = \arg((1 + i\beta \sin(\varphi))e^{-i\varphi/2})$, $i = \sqrt{-1}$, % means

remainder. The extraction coefficients to be modified are marked in Figure 11(d) with red;

- Update the affected edge and corner extraction coefficients. The edge point extraction coefficients are updated using Equation (3.1) - (3.2), and the corner point extraction coefficients are updated using Equation (3.3).

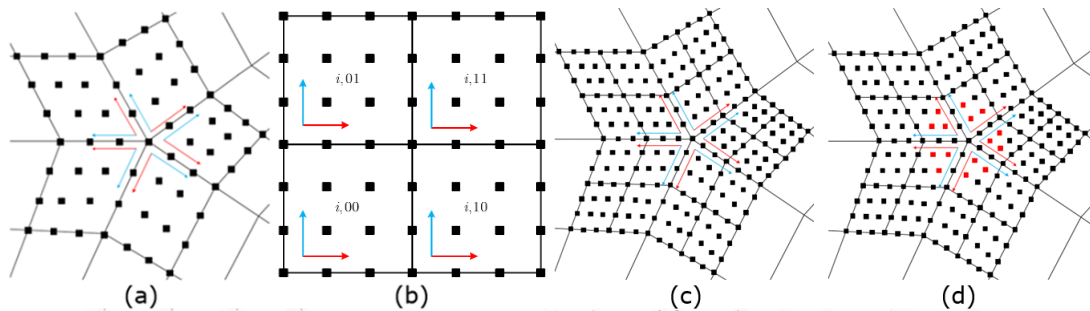


Figure 11: (a) Distribution of extraction coefficients on the irregular faces before splitting, (b) Numbering of the four sub-element domains, (c) Distribution of extraction coefficients on the irregular faces after splitting, (d) Extraction coefficients marked in red of the irregular faces that need to be changed to smooth spoke edges.

(2) In the analysis space, each irregular face introduces four face points. The transition point basis function T can be expressed as a linear combination^[2] as $T = \sum_{i=1}^{16} c_i m_i$, wherein m_i denotes

the face point basis function of the face that contact the transition point, c_i is called the face point coefficient. Among the 16 face point basis functions that represent the transition point basis function T , there must be irregular face's face point basis functions, which causes the reuse of these face point basis functions. To avoid this situation, the transition point basis function should be truncated and the contribution of irregular face's face point basis functions can thus be discarded, which means the face point coefficients of the truncated face point basis functions should be set to zero. Figure 12 shows some examples of basis function truncation.

In the analysis space, the algorithm is applied to irregular and transition faces, and the steps to obtain C^1 continuity crossing spoke edges are as follows:

- For an irregular or transition face, obtain all spline basis functions that have support on this face, and extraction matrix E . In the extraction matrix, set extraction coefficients defining the irregular point basis functions and transition point basis functions to zero.
- Truncate all transition point basis functions and irregular point basis functions, then the new extraction coefficients defining these spline basis functions will be found, and a new extraction matrix E defining this face will be obtained.
- Repeat the above two steps for each irregular face and transition face until the truncation is done and all new extraction matrix is obtained.
- The desired extraction matrix can be obtained by applying the algorithm in (1) to the irregular faces.

By executing these algorithms, the final continuity of the spline basis functions on the 2-disk faces of the extraordinary points is shown in Figure 13.

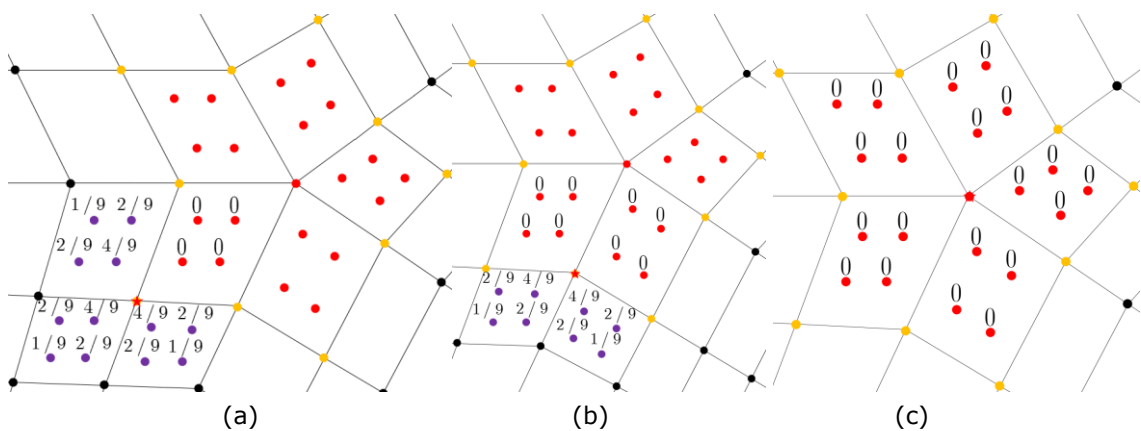


Figure 12: (a) and (b) are the truncation examples of two types of transition point basis functions respectively; (c) is the truncation example of extraordinary point basis functions. The points marked with red pentagram represent the spline basis functions to be analyzed, the purple face points represent the normal face point basis functions, and the red face points represent the face point basis functions that need to be discarded, of which the face point coefficients should be set to zero.

5 NUMERICAL EXAMPLE

As shown in Figure 14, we merge multiple NURBS surfaces into one single T-spline surface and use the above algorithm to enhance the continuity around extraordinary points. The T-spline surface is converted to a Bézier surface using Bézier extraction, and then an IGA simulation is performed on the model.

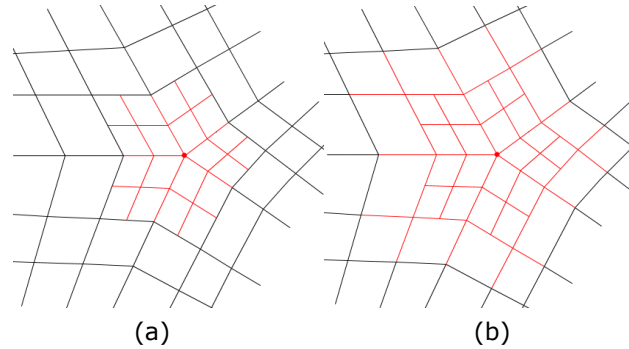


Figure 13: (a) and (b) are the continuity of the spline basis functions near extraordinary points in the design space and analysis space, respectively. Extraordinary point is marked in red, the spline basis functions across the red line have C^1 continuity, and the spline basis functions across the black line have C^2 continuity.

In this process, in order to avoid the problem that the adjacent edges of the 1-ring and 2-ring faces of the extraordinary point only have C^0 continuity, the transition faces and regular faces should be split. A distributed load downward on the top surface of the table model and a fixed constraint on the bottom edge are applied, and the material parameters are taken as: $E = 3 \times 10^{11}$, $\nu = 0.3$, $h = 0.03$, $F = 1.0$. An IGA simulation can be performed on this merged one-surface model, and Figure 15 shows the color plots of vertical displacement. This analysis case shows that the model after smoothing has C^1 continuity, and the continuity analyses of the merged surface before and after application of the continuity elevation algorithm are shown through the zebra pattern by Rhino in Figure 14(e)(f), which shows the continuity elevation clearly.

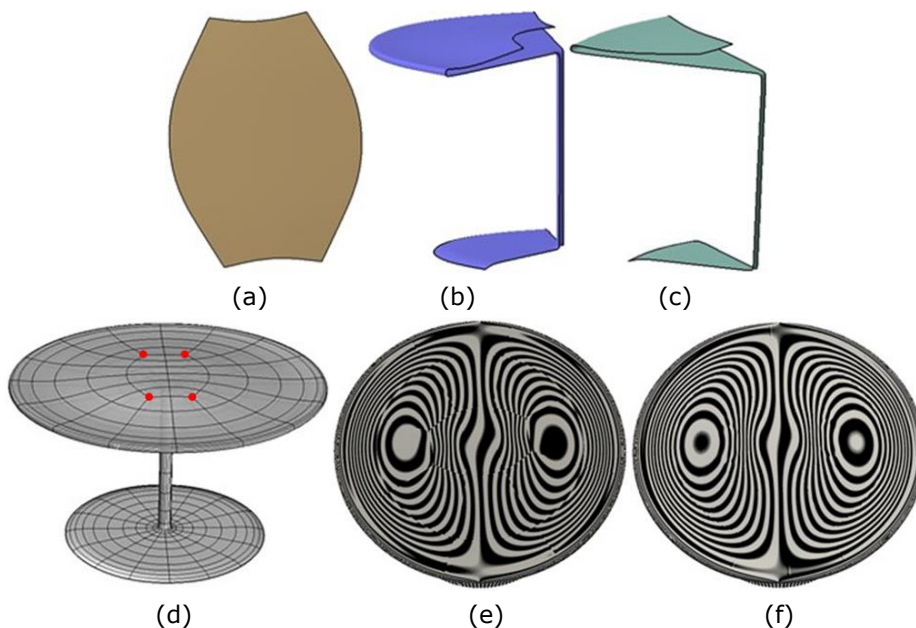


Figure 14: (a) (b) (c) are 3 NURBS surfaces, which can be used to merge into the table surface, of which surfaces in (b) and (c) are used twice; (d) Shows four extraordinary points marked in red on

the top surface of the model; (e) The zebra pattern on the top surface of the table before smoothing; (f) The zebra pattern on the top surface of the table after smoothing. We can see that: the zebra pattern near the extraordinary point before smoothing is discontinuous, indicating only C^0 continuity while the zebra pattern near the extraordinary point after smoothing is continuous but not smooth, indicating C^1 continuity.

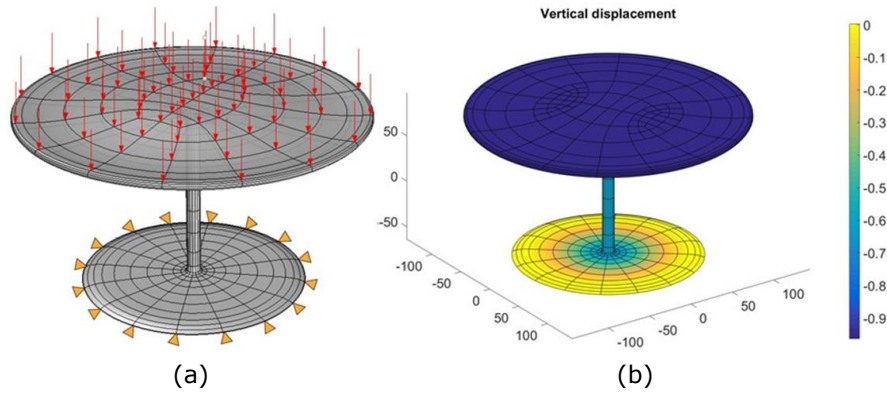
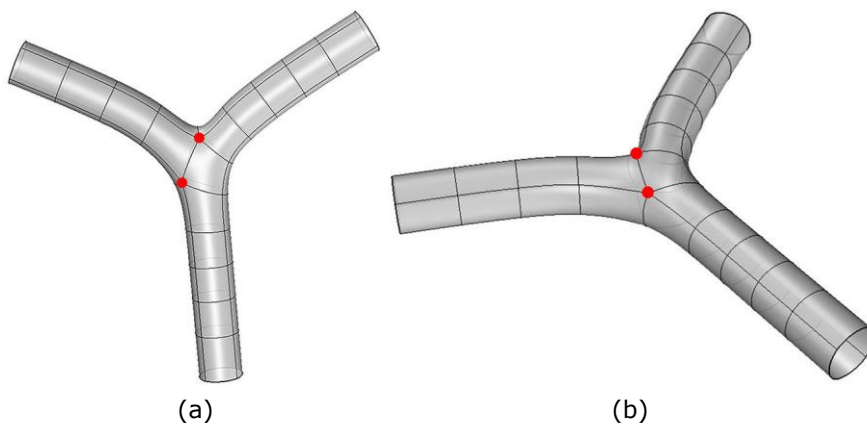


Figure 15: (a) Boundary conditions applied on the bottom side of the table, and distributed load applied on the top surface of the table, (b) Plot of the IGA simulation result of the table in vertical displacement.

As shown in Figure 16, a "Y"-shaped pipe model is given after surface merging and the above algorithm is used to enhance the continuity around extraordinary points. A concentrated force is applied on the upper right point of the pipe model and a fixed constraint is set on the bottom edge, the material parameters are taken as $E = 6.825 \times 10^7$, $\nu = 0.3$, $h = 0.04$, $F = 1.0$. An IGA simulation can be performed on this pipe model, and Figure 17 shows the color plots of vertical displacement. This analysis case shows that the pipe model after smoothing has C^1 continuity, and the continuity analyses of the pipe model before and after the continuity elevation algorithm are shown through the zebra pattern by Rhino in Figure 16(c)(d).



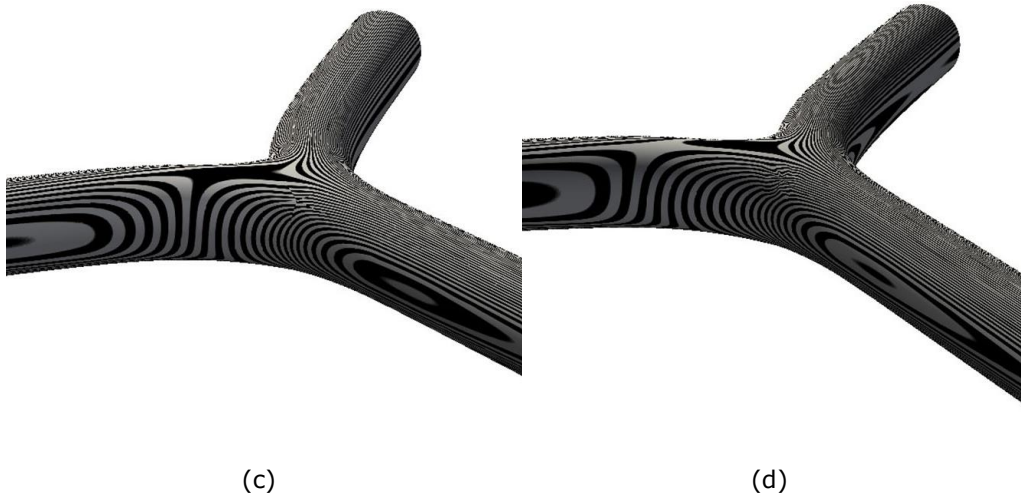
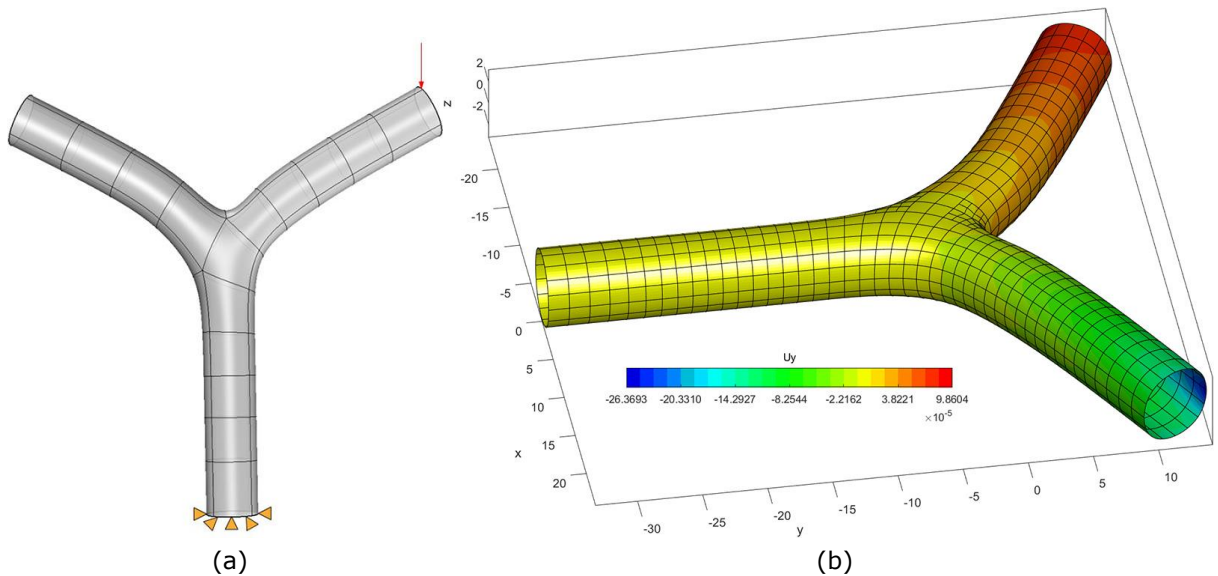


Figure 16: (a) and (b) are the “Y”-shaped pipe model with four extraordinary points marked with red, where the two extraordinary points on the back of the model are not shown; (c) The zebra pattern of the pipe model before smoothing; (d) The zebra pattern of the pipe model after smoothing. We can see that: the zebra pattern near the extraordinary point before smoothing is discontinuous and after smoothing becomes continuous, indicating the elevation from C^0 to C^1 continuity.



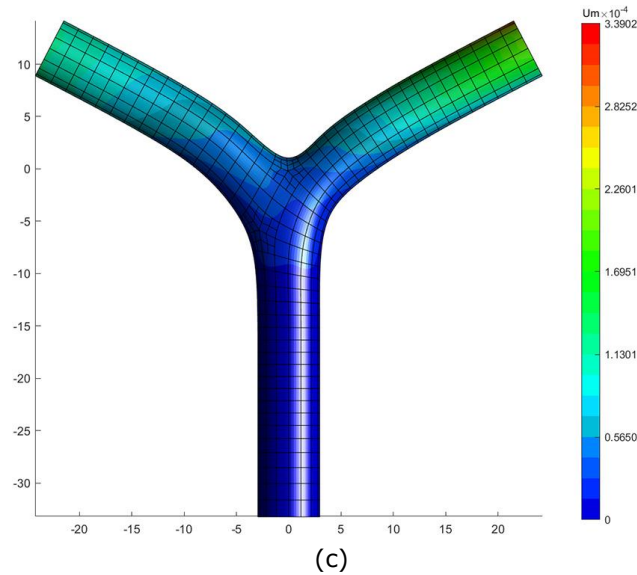


Figure 17: (a) Boundary conditions applied on the bottom side of the pipe model, and concentrated force applied on the upper right point of the pipe model; (b) Plot of the IGA simulation result of the pipe model in vertical displacement U_y ; (c) Plot of the IGA simulation result of the pipe model in vertical displacement U_m .

6 CONCLUSION

To enhance the spoke edge continuity that appears in unstructured T-spline surfaces, the design space and analysis space continuity enhancement algorithms are given in this paper. As shown in the use cases, when input multiple NURBS faces, they can be merged into one single unstructured T-spline surface, then the algorithm can be executed so that the spoke edges of extraordinary point obtain C^1 continuity. This procedure could be used to convert the existing multiple NURBS surface models into a T-spline surface model with at least C^1 inner continuity, which is easy to carry out IGA. With the technologies presented in this paper, more complex models from the design department are possible to be processed, thus offering a promising method to realize IGA scenarios in industry-level practices.

7 ACKNOWLEDGEMENTS

The work is supported by National Natural Science Foundation of China (Project Nos. 61972011, and 5217213).

REFERENCES

- [1] Borden, M.J.; Scott, M.A.; Evans, J.A.; Hughes, T.J.R.: Isogeometric finite element data structures based on Bézier extraction of NURBS, *International Journal for Numerical Methods in Engineering*, 87, 2011,15-47. <http://doi.org/10.1002/nme.2968>.
- [2] Casquero, H.; Wei, X.; Toshniwal, D.; Li, A.; Hughes, T.J.R.; Kiendl, J.; Zhang, Y.J.: Seamless integration of design and Kirchhoff-Love shell analysis using analysis-suitable

- unstructured T-splines, *Computer Methods in Applied Mechanics and Engineering*, 360, 2020,112756. <http://doi.org/10.1016/j.cma.2019.112765>.
- [3] Li, X.; Zheng, J.; Sederberg, T.W.; Hughes, T.J.R.; Scott, M.A.: On linear independence of T-spline blending functions, *Computer Aided Geometric Design*, 29, 2012,63-76. <http://doi.org/10.1016/j.cagd.2011.08.005>.
- [4] Nguyen, T.; Peter, J.: Refinable C1 spline elements for irregular quad layout, *Computer Aided Geometric Design*, 43,2016,123-130. <http://doi.org/10.1016/j.cagd.2016.02.009>.
- [5] Reif, U.: A Refinable Space of Smooth Surfaces of Arbitrary Topological Genus, *Journal of Approximation Theory*,90(2),1997,174-199. <http://doi.org/10.1006/jath.1996.3079>.
- [6] Scott, M.A.; Borden, M.J.; Verhoosel, C.V.; Sederberg, T.W.; Hughes, T.J.R.: Isogeometric finite element data structures based on Bézier extraction of T-spline, *International Journal for Numerical Methods in Engineering*,88,2011,126-156. <http://doi.org/10.1002/nme.3167>.
- [7] Scott, M.A.; Li, X.; Sederberg, T.W.; Hughes, T.J.R.: Local refinement of analysis-suitable T-spline, *Computer Methods in Applied Mechanics and Engineering*, 213-216, 2012, 206-222. <http://doi.org/10.1016/j.cma.2011.11.022>.
- [8] Scott, M.A.; Simpson, R.N.; Evans, J.A.; Lipton, S.; Boedas, S.P.A.; Hughes, T.J.R.; Sederberg, T.W.: Isogeometric boundary element analysis using unstructured T-splines, *Computer Methods in Applied Mechanics and Engineering*,254,2013,197-221. <http://doi.org/10.1016/j.cma.2012.11.001>.
- [9] Sederberg, T.W.; Cardonet, D.L.; Finnigan, G.T.; North, N.S.; Zheng, J.; Lyche, T.: T-spline simplification and local refinement, *ACM Transactions on Graphics*, 23(3), 2004,276-283. <http://doi.org/10.1145/1015706.1015715>.
- [10] Sederberg, T.W.; Zheng, J.; Bakenov, A.; Nasri, A.: T-spline and T_NURCCs, *ACM Transactions on Graphics*, 22(3), 2002,477-484. <http://doi.org/10.1145/882262.882295>.
- [11] Toshniwal, D.; Speleers, H.; Hughes, T.J.R.: Smooth cubic spline spaces on unstructured quadrilateral meshes with particular emphasis on extraordinary points: Geometric design and isogeometric analysis considerations, *Computer Methods in Applied Mechanics and Engineering*, 327, 2017, 411-458. <http://doi.org/10.1016/j.cma.2017.06.008>.
- [12] Wei, X.; Li, X.; Qian, K.; Hughes, T.J.R.; Zhang, Y.J.; Casquero, H.: Analysis-suitable unstructured T-splines: Multiple extraordinary point per face, *Computer Methods in Applied Mechanics and Engineering*,391,2022,114494. <http://doi.org/10.1016/j.cma.2021.114494>.